National assessment reveals widespread wind farm impacts on land surface temperature and vegetation in China

Geography and Sustainability 7 (2026) 100460

Contents lists available at ScienceDirect

Geography and Sustainability

journal homepage: www.elsevier.com/locate/geosus

Research Article

National assessment reveals widespread wind farm impacts on land surface temperature and vegetation in China

Ziyan Li[a,b], Yan Li[a,b,*], Yingzuo Qin[c], Laibao Liu[d,e], Eviatar Bach[f,g], Alona Armstrong[h,i], Guoqing Li[j], Mingquan Li[k,l], Zheng Wang[m,n], Yongqing Bai[o], Zhengchao Chen[o]

[a] State Key Laboratory of Earth Surface Processes and Hazards Risk Governance, Faculty of Geographical Science, Beijing Normal University, Beijing 100875, China
[b] Institute of Land Surface System and Sustainable Development, Faculty of Geographical Science, Beijing Normal University, Beijing 100875, China
[c] School of Environmental Science and Engineering, Southern University of Science and Technology, Shenzhen 518055, China
[d] Department of Geography, The University of Hong Kong, Hong Kong 999077, China
[e] Institute for Climate and Carbon Neutrality, The University of Hong Kong, Hong Kong 999077, China
[f] Department of Meteorology and Department of Mathematics and Statistics, University of Reading, Reading, United Kingdom
[g] National Centre for Earth Observation, Reading, United Kingdom
[h] Lancaster Environment Centre, Lancaster University, Lancaster LA14YQ, United Kingdom
[i] Energy Lancaster, Lancaster University, Lancaster LA14YW, United Kingdom
[j] School of Resources and Environmental Engineering, Ludong University, Yantai 264025, China
[k] School of Economics and Management, Beihang University, Beijing, China
[l] MOE Laboratory for Low-carbon Intelligent Governance (LLIG), Beihang University, Beijing, China
[m] Bay Area International Business School, Beijing Normal University at Zhuhai, Zhuhai 519087, China
[n] Harvard-China Project on Energy, Economy and Environment, Harvard John A. Paulson School of Engineering and Applied Sciences, Harvard University, Cambridge, MA, 02138, USA
[o] State Key Laboratory of Remote Sensing and Digital Earth, Aerospace Information Research Institute, Chinese Academy of Sciences, Beijing 100101, China

HIGHLIGHTS

- The 675 wind farms in China exhibiteda consistent pattern of nighttime warming and daytime cooling in LST.
- Vegetation index decreased due to wind farm construction and recovered over time.
- Wind farm impacts on LST and vegetation varied by land cover type.
- Land cover distributions contributed to the latitudinal variations of nighttime LST impacts.

GRAPHICAL ABSTRACT

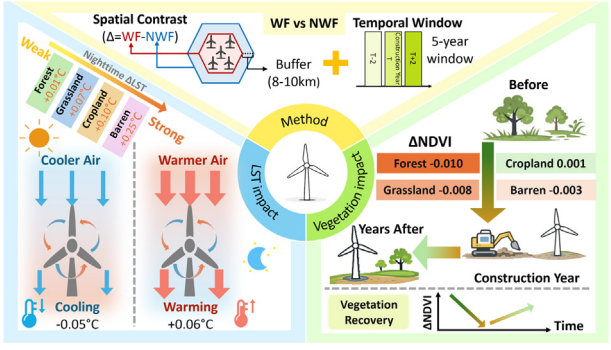

ARTICLE INFO

Article history:
Received 20 December 2024
Received in revised form 8 March 2026
Accepted 8 March 2026
Available online 11 March 2026

ABSTRACT

The rapid development of wind energy in China since 2000 has raised concerns about its impacts on local climate and vegetation. Despite regional and local studies, a comprehensive national assessment is lacking. Here, we analyzed the effects of 675 onshore wind farms, representing >90,000 identified wind turbines in China, on land surface temperature (LST) and vegetation using Moderate-resolution Imaging Spectroradiometer (MODIS) satellite data from 2003 to 2022. We found a daytime cooling effect of -0.05 ± 0.48 °C (mean ± STD) and a nighttime warming effect of 0.06 ± 0.28 °C across all wind farms. The construction of wind farm infrastructure initially reduced peak normalized difference vegetation index (NDVI) by -0.006 ± 0.036, and this adverse impact weakened over time (-0.004 after 7 years), indicating vegetation recovery. The wind farm impacts varied by land cover type. The nighttime warming was largest for barren lands (0.19 °C), followed by croplands (0.10 °C), grasslands (0.07 °C), and forests (0.01 °C). These differences contributed to increasing night warming from southern

* Corresponding author.
E-mail address: yanli.geo@gmail.com (Y. Li).

https://doi.org/10.1016/j.geosus.2026.100460

Keywords:
Wind farm
LST
Vegetation
Land cover
NDVI
Environmental impact

to northern China. The adverse vegetation impacts were largest for forests (-0.010), followed by grasslands (-0.008) and barren lands (-0.003), with croplands (0.001) being almost unaffected. Correlation analysis identified precipitation and mean LST as significant factors influencing spatial variations in nighttime LST impact, with greater vegetation decline reinforcing night warming. Our large-scale analysis provides comprehensive evidence of the heterogeneous environmental impacts of wind farms across China, informing the sustainable development of wind energy.

1. Introduction

To mitigate climate change and reduce carbon emissions from fossil fuels, countries worldwide have been accelerating the growth of renewable energy, particularly wind and solar power. With 1,174 gigawatts of installed capacity by the end of 2024, the world's wind power capacity now meets around 10 % of global electricity demand (World Wind Energy Association, 2025). China has played a dominant role in global wind power development, with fast growth since the beginning of the 21st century. China's cumulative installed wind power capacity reached 561 gigawatts by 2024, accounting for 47.8 % of the global total and ranking among the highest annual growth rate (18.3 %) among major markets (World Wind Energy Association, 2025).

Despite the benefits of carbon reduction, wind energy development has ecological and climatic consequences through the construction and operation of wind farms. Research has explored wind farm impacts at local, regional, and global scales through field observations (Armstrong et al., 2014; Baidya Roy and Traiteur, 2010), remote sensing (Luo et al., 2021; Roy et al., 2004; Zhou et al., 2012) and numerical model simulations (Fiedler and Bukovsky, 2011; Li et al., 2018; Miller and Keith, 2018; Pan and Archer, 2018). Wind turbines, established as momentum sinks and turbulence sources, enhance the mixing of the atmospheric boundary layer through the rotation of their blades, bringing air from the upper layer to warm the surface (Armstrong et al., 2014; Baidya Roy and Traiteur, 2010; Zhou et al., 2012). The surface warming effect is stronger under stable atmospheric conditions, for example, at night (Zhou et al., 2012), since the potential temperature increases with height under stable boundary layer conditions. During the day, with vigorous convection activities, the turbulence generated by the blades is negligible relative to the background turbulence, and the airflow brought down may not be able to heat the ground surface. Generally, a strong warming effect at night and a weak cooling effect during the day occur, regardless of location around the world and the choice of method (Liu et al., 2022; Miller and Keith, 2018; Qin et al., 2022; Baidya Roy and Traiteur, 2010; Slawsky et al., 2015; Tang et al., 2017; Wu et al., 2019; Zhang et al., 2023). For example, using MODIS remote sensing data, Zhou et al. (2012) found that the land surface temperature in the wind farm area of Texas, US, increased by 0.31–0.71 °C at night, but no noticeable change was observed during the day. Moreover, the magnitude of surface temperature changes induced by wind farms is reportedly related to wind speed, as the highest wind speed in a western Texas wind farm was found to explain the strongest night warming in summer (Zhou et al., 2013).

Studies have also explored the seasonal variations in temperature effects of wind farms. Zhou et al. (2013) analyzed the daily and seasonal variations of wind farm impacts and found that their influence on temperature was greater in summer than in winter. Chang et al. (2016) analyzed the MODIS LST at the Guazhou wind farm in China from 2005 to 2012 and reported the strongest warming during the summer night (0.51 °C). Another study in west-central Texas found that the turbine-induced turbulence relative to the background turbulent kinetic energy (TKE) can explain most of the diurnal and seasonal variations in nighttime LST effects (Xia et al., 2016).

Wind farms across different land cover types showed distinct nighttime warming effects (Qin et al., 2022). Most studies include only a limited number of land cover types, and few provide comparisons across diverse land cover types. The primary focus of existing studies in China is on deserts, grasslands, and croplands, with the strongest warming effect often found in deserts (Chang et al., 2016; Liu et al., 2024, 2023, 2022; Luo et al., 2021; Su et al., 2024; Wang et al., 2019; Zhang et al., 2023). Research on forest wind farms has also emerged in recent years, focusing on fine-scale impacts or the influence of complex terrain (Li et al., 2024; Ma et al., 2023; Xia et al., 2025).

Wind turbines in operation can alter air temperature and humidity, with potential consequences for soil moisture and fertility, both of which affect local vegetation growth (Diffendorfer et al., 2022; Luo et al., 2021; Xu et al., 2019). It is reported that reduced soil moisture caused by the warming effects of wind farms in Northern China may decrease vegetation in arid and semi-arid regions (Liu et al., 2024; Tang et al., 2017; Wang et al., 2023). Furthermore, remote sensing analysis of the Bashang wind farm in northern China revealed inhibitory effects on vegetation in summer due to suppressed soil moisture and exacerbated water stress (Tang et al., 2017). In contrast, another field study in China's Gobi desert found greater plant physiological state, higher plant density, and higher above-ground biomass in wind farm areas (Xu et al., 2019).

Wind farms also directly affect local vegetation during construction. Road construction and wind turbine installations break the surface morphology and remove vegetation, resulting in reduced vegetation and barren soil (Aksoy et al., 2023; Li et al., 2024; Ma et al., 2023; Urziceanu et al., 2021). The destruction of vegetation can lead to changes in soil physical and chemical properties (Li et al., 2024), thereby reducing soil fertility and affecting vegetation growth. Although these direct effects are confined to wind farm locations (Aksoy et al., 2023), they may have long-lasting impacts on vegetation growth and plant diversity. A field survey in Romania revealed that species richness, affected by wind power construction, did not recover after 10 years of restoration and protection (Urziceanu et al., 2021). However, the long-term vegetation recovery has been observed in wind farms in Hebei and Hunan, China (Li et al., 2024; Luo et al., 2021). The indirect impacts on local vegetation through changes in microclimate are compounded with direct impacts, making them difficult to distinguish (Diffendorfer et al., 2022; Qin et al., 2022; Tang et al., 2017). Given these inconsistent findings, it is necessary to assess the effects on vegetation and their variations by studying additional wind farms with different attributes and operating in different climatic and geographic environments.

Existing studies in China have primarily focused on individual or a few large wind farms at local or regional scales (e.g., Northern China), yielding inconsistent results (Liu et al., 2021; Xia et al., 2016; Xu et al., 2019; Zhang et al., 2023). A comprehensive assessment for China remains lacking (Liu et al., 2023, 2022; Tang et al., 2017; Wang et al., 2019). Remote sensing satellites such as MODIS and Landsat offer various data products for land cover, land surface temperature, and vegetation index, which enable monitoring of land cover changes, wind farm-induced local climate and vegetation impacts at regional and global scales (Hou et al., 2025; Li et al., 2024; Liu et al., 2023, 2022; Luo et al., 2021; Qin et al., 2022). This study aims to quantify the impacts of 675 wind farms on land surface temperature and vegetation in China, using MODIS data, and to explore spatial patterns and driving factors. Specifically, we first quantified the impacts of wind farms on land surface temperature, their seasonal variations, and their dependence on land cover. Next, we analyzed peak NDVI to assess the impacts of wind farms on different vegetation types and their recovery over time. Finally, we conducted correlation analyses to explore the environmental factors influencing spatial patterns of wind farm impacts in China and

to provide explanations for potential mechanisms. Our comprehensive national-level assessment, utilizing wind farm samples from diverse climate zones and vegetation types, can enhance the representativeness of the detected wind farm impacts.

2. Materials and methods

2.1. Data

2.1.1. Wind turbine data

The geographical locations of wind turbines used in this study were extracted from the GF1/2 data in 2019 using the deep learning object detection algorithm You Only Look Once (YOLO) (Redmon et al., 2016). YOLO has been demonstrated to accurately detect the position of a wind turbine from images with multiple backgrounds and resolutions (Zhai et al., 2024), enabling the identification of more than 90,000 individual turbines in China. These wind turbines were first aggregated into 869 clusters using a Density-Based Spatial Clustering of Applications with Noise (DBSCAN) algorithm from the *scikit-learn* package in Python, with the criteria of 1) the distance between each turbine must be smaller than 0.1°, and 2) a minimum of 5 turbines for each wind farm cluster. Each wind turbine cluster was treated as a wind farm.

All wind farm clusters were visually verified using Google Earth imagery to remove misclassified clusters, resulting in a total of 814 verified wind farms. The construction year of each wind farm was manually determined by the timestamps of two Google Earth images: the earliest one in which wind turbines first appeared and the next available one in which over half of the turbines were constructed. Since the identified timestamps may span several years, the middle year between the two was assigned as the wind farm's build year of. Due to blurring, missing, and cloudy images, only 678 wind farms were assigned valid construction years from 2006 to 2020. After discarding three wind farms that displayed null LST and NDVI values, 675 wind farms were retained for analysis (Table S1 in the Supplementary materials).

2.1.2. Land cover data

This study used MODIS land cover data from 2019 (MCD12Q1.061) based on International Geosphere-Biosphere Program (IGBP) classifications at 500 m resolution, obtained from Google Earth Engine (GEE). To determine the land cover type for each wind farm, we extracted the land cover at each turbine location and used the majority type as the wind farm's land cover. The extracted 13 IGBP land cover types were grouped and reclassified into 6 types: barren, croplands, grasslands, forests, wetlands, and impervious surfaces (Table S2 in the Supplementary materials).

2.1.3. Environmental and climatic data

We obtained LST, NDVI, and other environmental data from GEE. The MODIS LST data product from Aqua (MYD11A2.061), which has a spatial resolution of 1 km and a temporal resolution of 8 days, was used to quantify the impacts of wind farms on land surface temperature. The MODIS NDVI data product from Aqua (MYD13A2.061) at 1 km resolution with a 16-day temporal resolution was used to quantify vegetation impacts. Additionally, MODIS LST and NDVI data products from Terra satellite (MOD11A2.061 & MOD13A2.061) were used to verify the results. The MODIS LST data include two local overpass times, 1:30 and 13:30 for Aqua and 10:30 and 22:30 for Terra. We used the LST product from the Aqua satellite to approximate the maximum and minimum temperatures of a day. The average NDVI from the Aqua and Terra satellites was computed to reduce data uncertainty. Both LST and NDVI datasets span from 2003 to 2022.

To explore the spatial variations in wind farm impacts, we selected several climate variables as candidate influencing factors, including precipitation and evapotranspiration from the ERA5 Land reanalysis (Hersbach et al., 2020), with a spatial resolution of 0.1° and covering the period from 2003 to 2022. Since there were only 10 m wind velocity data available on GEE in ERA5 Land reanalysis, to be more consistent with the height of the wind hub, we chose wind velocity at 50 m from the Modern-Era Retrospective analysis for Research and Applications Version 2 (MERRA-2) datasets (Gelaro et al., 2017) with a spatial resolution of 0.625° by 0.5°. Digital elevation model data were from the Shuttle Radar Topography Mission (SRTM) V3 at a 90 m resolution in 2000.

2.2. Methods

2.2.1. Quantifying wind farm impacts

Following Qin et al. (2022), the wind farm impacts were quantified by differences in changes of the variable of interest (e.g., LST or NDVI) between wind farm locations and their surrounding areas during a period before and after their construction. These differences are attributed to the influence of wind farms, assuming wind farms and their surrounding areas share similar background climatic and environmental conditions. For each wind farm, pixels with wind turbines were identified as the wind farm area (WF). Since wind farm impacts on LST spread downwind and decrease with distance, we created a buffer zone 8–10 km from the WF as the non-wind farm (NWF) reference area (a schematic of the NWF is shown in Fig. S1 in the Supplementary materials). This reference zone was chosen based on our previous findings that the NWF, located 8–10 km away, has similar climatic conditions to WF but is under minimal wind farm influence (Qin et al., 2022). The workflow for this data processing and analysis is given in Fig. S2 in the Supplementary materials.

The wind farm impacts were quantified as the differences in LST or NDVI changes between WF and NWF during a time window centered on the build year. Precisely, the LST impact (ΔLST) is estimated by Eq. (1):

$$\Delta LST = \Delta LST_{WF} - \Delta LST_{NWF} = LST_{Trend_{WF}} \times \Delta T - LST_{Trend_{WF}} \times \Delta T \quad (1)$$

where ΔLST_{WF} and ΔLST_{NWF} are temporal LST changes over WF and NWF areas, respectively, which were estimated by their linear trends per unit time ($LST_{Trend_{WF}}$ and $LST_{Trend_{NWF}}$) during the time window multiplied by the length of the time window (ΔT). ΔLST can be estimated at annual or seasonal scales.

For vegetation impacts, we calculated the 95th percentile of 16-day NDVI within a year as peak NDVI in the growing season and then quantified wind farm impact (ΔNDVI) following Eq. (2), similar to ΔLST:

$$\begin{aligned}\Delta NDVI &= \Delta NDVI_{WF} - \Delta NDVI_{NWF} \\ &= NDVI_{Trend_{WF}} \times \Delta T - NDVI_{Trend_{WF}} \times \Delta T\end{aligned} \quad (2)$$

Trend estimation and its time window are critical in quantifying the impact of wind farms. We chose a 5-year window (i.e., two years before and after the build year) to estimate the temporal changes caused by wind farms. Including the build year as the middle of the time window can capture the changes before and after the construction of a wind farm. In contrast to subtracting the first year from the last, using trend terms reduces the influence of interannual fluctuations. Sensitivity to alternative time window lengths was also tested, and the results were reported in the discussion. The trend terms were estimated using the *polyfit* function, in the *NumPy* package of Python. Additionally, a one-sample *t*-test was conducted to assess the statistical significance of the estimated wind farm effects relative to zero.

2.2.2. Correlation analysis for spatial variations of wind farm impacts

We conducted a Pearson correlation analysis using the *scipy* package's *pearsonr* function in Python to explore the spatial relationships between wind farm impacts and various environmental factors. Environmental factors include turbine counts, 50 m wind velocity, longitude, latitude, altitude, the altitude difference between WF and NWF, slope,

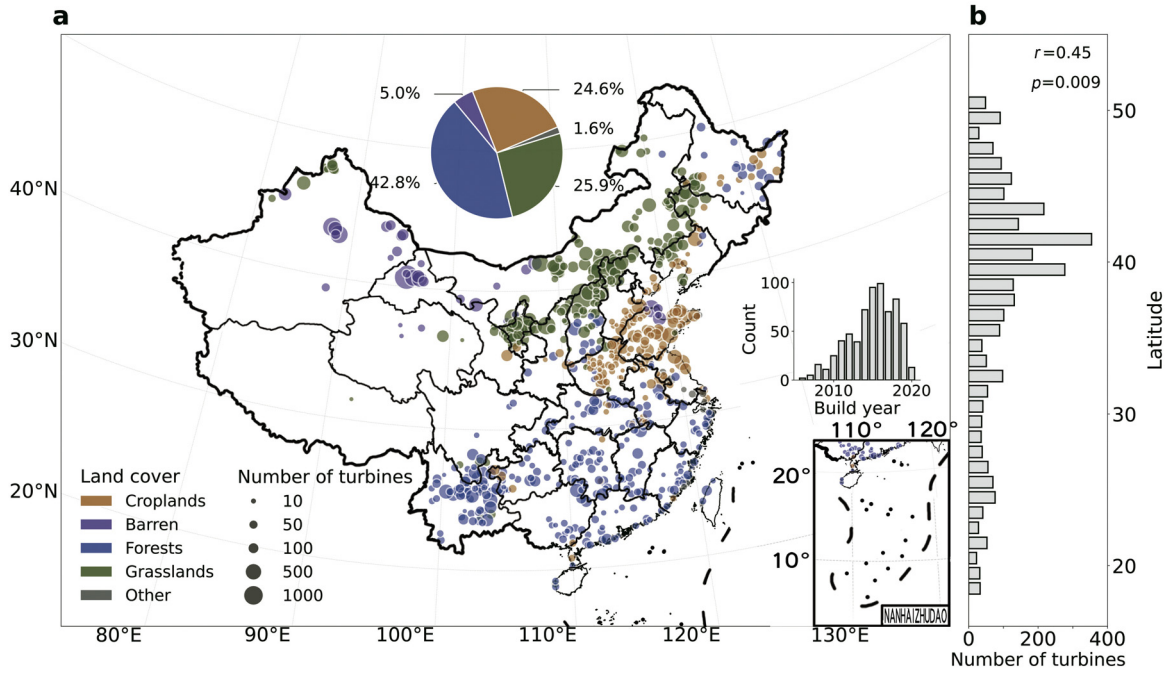

Fig. 1. Spatial distribution and latitudinal variations of 675 wind farms in China. (a) Spatial distribution of 675 wind farms in China. The size of the point on the map represents the number of turbines in each wind farm, while the color indicates the type of land cover. The pie chart illustrates the proportion of each land cover type. The histogram illustrates the number of wind farms constructed annually from 2006 to 2020. (b) The average number of turbines in wind farms across each 1° latitude band.

precipitation, evapotranspiration, LST, and NDVI. All these factors were calculated by spatial averaging at each WF location for time-invariant variables and by temporal averaging over the time window for time-varying variables, such as 50 m wind velocity, precipitation, evapotranspiration, LST, and NDVI.

2.2.3. Decomposition of latitudinal variations of wind farm impacts

There are significant variations of wind farm impacts across land cover types (Qin et al., 2022), while the latitudinal distribution of land cover in China is characterized by more forests in the south and more grasslands and barren lands in the north. To determine how land cover distribution may contribute to latitudinal variations in wind farm impacts, we applied a decomposition method to separate latitudinal LST impacts into those induced by land cover distribution, by wind farms of specific land cover, and by their interactions across latitudes. Suppose that the mean ΔLST at latitude band lat, ($\overline{\Delta LST_{lat}}$) can be represented as the weighted mean of ΔLST of wind farms under different land cover types ($\overline{\Delta LST_{lat,lc}}$) and the weights are the proportions of each land cover within the latitude band lat ($\sum_{lc} R_{lat,lc} = 1$) (Eq. (3)).

$$\overline{\Delta LST_{lat}} = \sum_{lc} \left(\overline{\Delta LST_{lat,lc}} \times R_{lat,lc} \right) \tag{3}$$

where $\overline{\Delta LST_{lat,lc}}$ is the mean ΔLST of wind farms of land cover type lc (lc∈ (barren, croplands, grasslands, and forests)) at latitude band lat, and $R_{lat,lc}$ is the proportion of land cover lc in all wind farms at the latitude band lat.

For a specific land cover type lc, $\overline{\Delta LST_{lat,lc}}$ and $R_{lat,lc}$ can be written as a mean value of all latitude bands and a deviation term at latitude band lat ($\overline{\Delta LST_{lat,lc}} = \overline{\Delta LST_{lc}} + \delta\Delta LST_{lat,lc}$; $R_{lat,lc} = \overline{R_{lc}} + \delta R_{lat,lc}$). Eq. (4) can be rewritten as:

$$\begin{aligned}\overline{\Delta LST_{lat}} = \sum_{lc} \Big(& \overline{\Delta LST_{lc}} \times \overline{R_{lc}} + \overline{\Delta LST_{lc}} \times \delta R_{lat,lc} + \overline{R_{lc}} \times \delta\Delta LST_{lat,lc} \\ & + \delta\Delta LST_{lat,lc} \times \delta R_{lat,lc} \Big) lc \\ & \in \{\text{barren, croplands, grasslands, forests}\}\end{aligned} \tag{4}$$

Combining corresponding terms of land cover types yielded Eq. (5) with ΔLST at each latitude decomposed into four terms:

$$\begin{aligned}\overline{\Delta LST_{lat}} = & \sum_{lc} \left(\overline{\Delta LST_{lc}} \times \delta R_{lat,lc} \right) + \Bigg(\sum_{lc} \left(\overline{\Delta LST_{lc}} \times \overline{R_{lc}} \right) \\ & + \sum_{lc} \left(\delta\Delta LST_{lat,lc} \times \overline{R_{lc}} \right) + \sum_{lc} \left(\delta\Delta LST_{lat,lc} \times \delta R_{lat,lc} \right) \Bigg), \ lc \\ & \in \{\text{barren, croplands, grasslands, forests}\}\end{aligned} \tag{5}$$

Therefore, the latitudinal ΔLST can be decomposed to latitudinal changes induced by land cover distribution ($\sum_{lc}(\overline{\Delta LST_{lc}} \times \delta R_{lat,lc})$), and the rest referring to non-land cover terms is the sum of 1) mean LST impact ($\sum_{lc}(\overline{\Delta LST_{lc}} \times \overline{R_{lc}}) = \overline{\Delta LST}$), 2) latitudinal changes induced by latitude but not land cover type ($\sum_{lc}(\delta\Delta LST_{lat,lc} \times \overline{R_{lc}})$), 3) and their interactions ($\sum_{lc}(\delta\Delta LST_{lat,lc} \times \delta R_{lat,lc})$) (Fig. S3 in the Supplementary materials).

3. Results

3.1. Spatial distribution of wind farms and their characteristics

A total of 675 wind farms with valid build years and LST and NDVI values were selected from 869 wind farm samples for our analysis. According to the build-year distribution, wind farms in China have experienced rapid growth since 2000, particularly after 2013, when 78 % of wind farms were built. The wind farms were primarily located in eastern China, with larger farms concentrated in the northwest and few on the Tibetan plateau (Fig. 1a). Four land cover types were distributed among wind farms, including forests (42.8 %) mainly in south China, grasslands (25.9 %) in the mountainous regions and the Mongolian Plateau, croplands (24.6 %) in the North China Plain, and barren lands (5.0 %) in the arid areas of Northwest China. The wind farm size, defined as the number of turbines per farm, showed a latitudinal distribution, with larger farms in the north and smaller ones in the south (Fig. 1b).

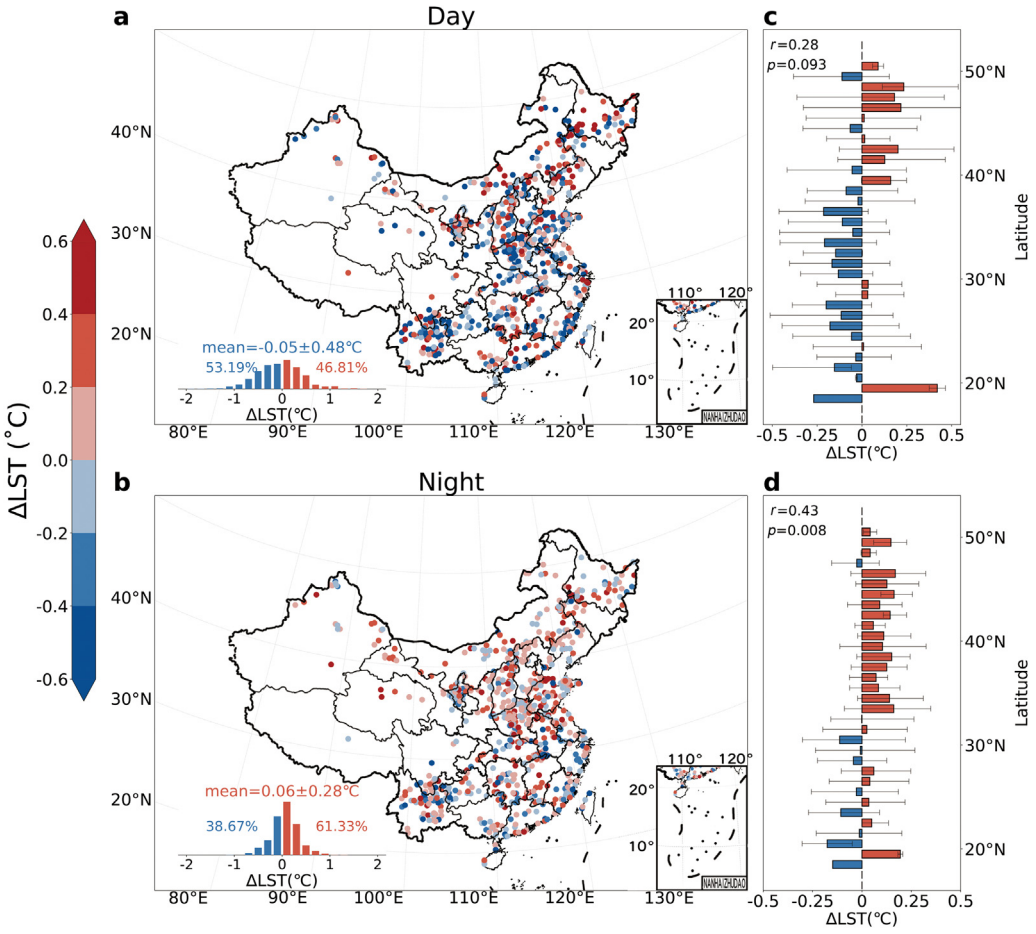

Fig. 2. Wind farm impacts on annual mean daytime (a) and nighttime LST (b) (ΔLST) and their latitudinal variations (c, d). The insets in panels a and b show the histogram of ΔLST for 675 wind farms with mean values and percentages of positive (red) and negative (blue) values. Grey error lines in panels c and d represent the range from the 25th to 75th percentile at each latitude band. A Pearson correlation test is performed between latitude and the mean LST effect at each latitude.

3.2. Impacts on land surface temperature

Fig. 2 shows the diurnally asymmetric impacts of 675 wind farms on LST in China, indicating significant nighttime warming effects, but weak daytime effects. During the daytime, wind farms showed an annual mean ΔLST of −0.05 ± 0.48 °C ($p < 0.01$; *t*-test), indicating an overall cooling effect. However, the spatial pattern of daytime ΔLST was heterogeneous, with warming (positive ΔLST) and cooling (negative ΔLST) effects close in proportion (53.19 % vs. 46.81 %) and no significant latitudinal pattern ($r = 0.28$, $p = 0.093$; Fig. 2c). At night, the annual mean ΔLST was 0.06 ± 0.28 °C ($p < 0.01$) across 675 wind farms, with positive ΔLST in 61.33 % of wind farms, indicating a predominant nighttime warming effect. Spatially, nighttime ΔLST increased with latitude ($r = 0.43$, $p < 0.01$; Fig. 2d), suggesting a stronger warming in northern China.

To investigate seasonal variations, we estimated ΔLST for spring (March to May), summer (July to August), autumn (September to November), and winter (December to February), respectively. For daytime ΔLST, spring was the only season with a statistically significant cooling effect (−0.10 ± 0.89 °C, $p < 0.01$), while in the other three seasons, the effects were not significant (Fig. S4 in the Supplementary materials). In contrast, nighttime warming effects on LST were significant in most seasons, except summer (0.01 ± 0.48 °C, $p = 0.44$). Autumn had the strongest warming effect of 0.11 ± 0.50 °C ($p < 0.01$) (Fig. 3), followed by winter (0.07 ± 0.57 °C, $p < 0.01$) and spring (0.06 ± 0.52 °C, $p < 0.01$). The latitudinal pattern of nighttime ΔLST was most evident in winter ($p < 0.01$) (Fig. S5 in the Supplementary materials), indicating a stronger warming effect at higher latitudes.

Land cover strongly influenced wind farm's effect on LST. The annual mean nighttime ΔLST ranked as barren lands (0.25 °C) > croplands (0.10 °C) > grasslands (0.07 °C) > forests (0.01 °C) (Fig. 4). The strongest warming in barren land persisted in four seasons (ranging from 0.25 °C to 0.29 °C). Despite the overall minor LST impacts in summer ($|\Delta LST| \leq 0.01$ °C), wind farms in croplands (0.09 °C to 0.18 °C) and grasslands (0.08 °C to 0.11 °C) showed significant warming in the other three seasons. For forest wind farms, the signs of impacts varied seasonally, from significant warming in autumn (0.10 °C) to weak cooling in spring (−0.02 °C) and winter (−0.02 °C). This may be related to the higher background surface roughness of forests, which produces stronger turbulence than other land cover types, leading to weaker atmospheric stratification and, consequently, a weaker LST effect (Kirk-Davidoff and Keith, 2008; Qin et al., 2022).

3.3. Impacts on vegetation

Wind farm impacts on local vegetation were quantified using peak NDVI (ΔNDVI). A noticeable overall decrease in peak NDVI with a mean magnitude of −0.006 ± 0.036 ($p < 0.01$) was observed across all 675 wind farm samples (Fig. 5), indicating an adverse effect on local vegetation probably due to vegetation removal by turbine installation and road construction (Li et al., 2024; Ma et al., 2023; Xia et al., 2025). Despite the adverse effects of 56.4 % of wind farms, 43.6 % showed a positive vegetation effect, which could be related to vegetation recovery after construction (Li et al., 2024; Luo et al., 2021). Additionally, the spatial distribution of vegetation impact was heterogeneous and did not show a dependence on latitude ($r = -0.12$, $p = 0.515$).

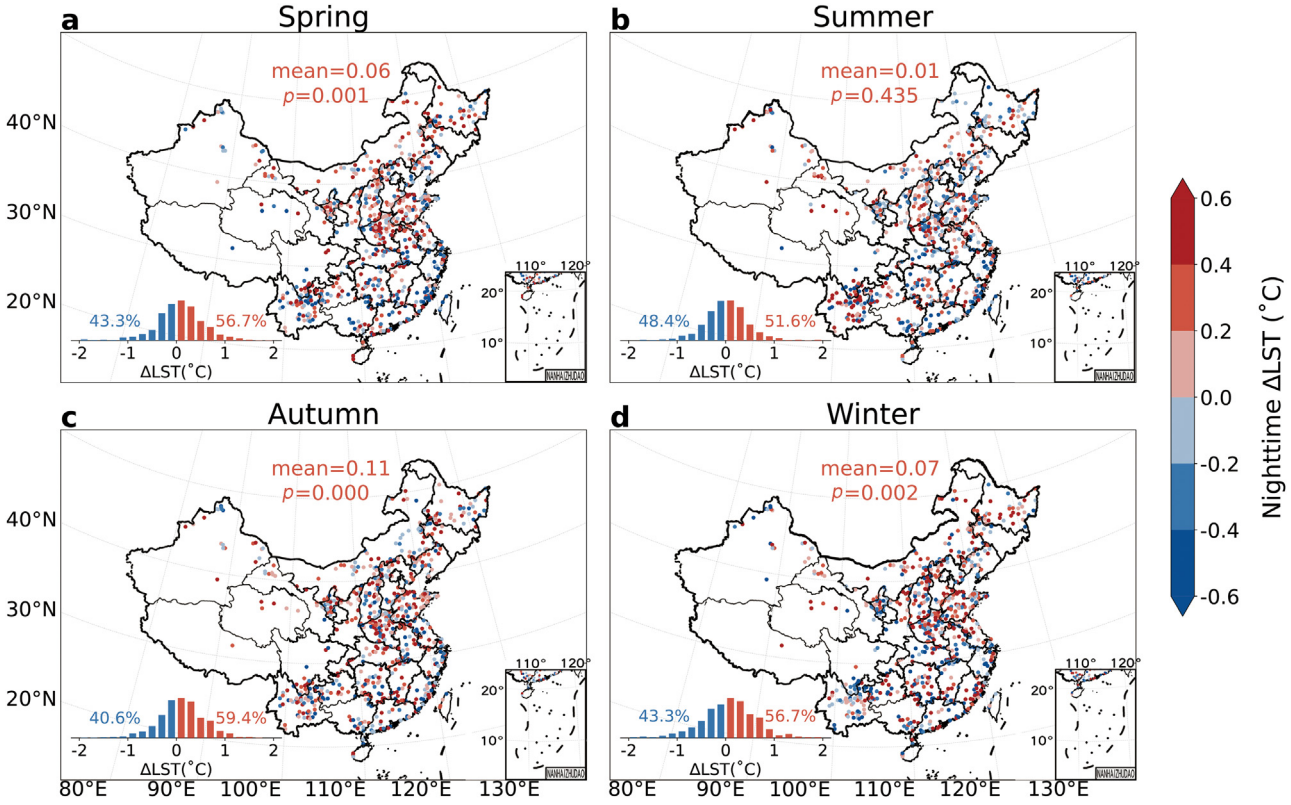

Fig. 3. Seasonal variations of wind farm impacts on nighttime LST (ΔLST) in spring (a), summer (b), autumn (c), and winter (d).

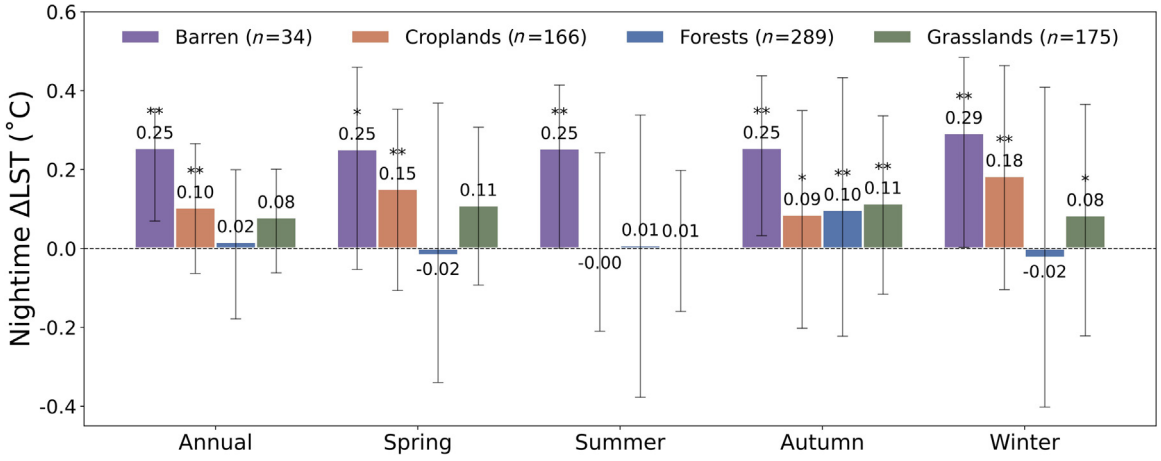

Fig. 4. Annual and seasonal nighttime ΔLST of wind farms for different land cover types (barren, croplands, forests, and grasslands). Numbers with asterisks indicate statistical significance calculated using a *t*-test (** for $p < 0.01$, * for $p < 0.05$, and no mark for $p \geq 0.05$). Grey error bars represent the interquartile range.

The impacts of wind farms on local vegetation showed notable differences across different land cover types. The adverse vegetation impacts were particularly severe in forests (ΔNDVI = −0.0102, $p < 0.01$, 61.6 % negative) and grasslands (−0.0079, $p < 0.01$, 57.7 % negative) (Fig. 6a). The greater vegetation loss was associated with the land cover's high NDVI. With low background NDVI (0.0616), wind farms on barren land caused an insignificant decrease in peak NDVI (−0.0026, 61.8 % negative). Although croplands had a high background NDVI (0.4501), the vegetation effect was negligible (0.0006, 53.6 % positive). The weak positive vegetation effect on croplands may be related to rapid vegetation recovery, as crops are replanted annually, or to the use of crop field paths during wind turbine construction, which helps avoid vegetation removal. When the time window extends, ΔNDVI on barren lands and grasslands slightly declined while rapidly increasing on croplands and forests (Fig. 6b), indicating vegetation recovery since wind farm construction. With a longest 17-year window, the negative impact on forests was negligible.

3.4. Spatial variations of wind farm impacts and their influencing factors

We conducted a correlation analysis to explore spatial variations in wind farm impacts and their influencing factors (Fig. 7a). Correlations for LST impacts were similar between nighttime and daytime ΔLST, but stronger at night. There were significant negative correlations between nighttime ΔLST and slope (−0.11), altitude difference (−0.10), and NDVI (−0.09), suggesting weaker nighttime warming in wind farms with more complex terrain (characterized by higher altitude, larger altitude differences, and steeper slopes) and lusher vegetation. In partic-

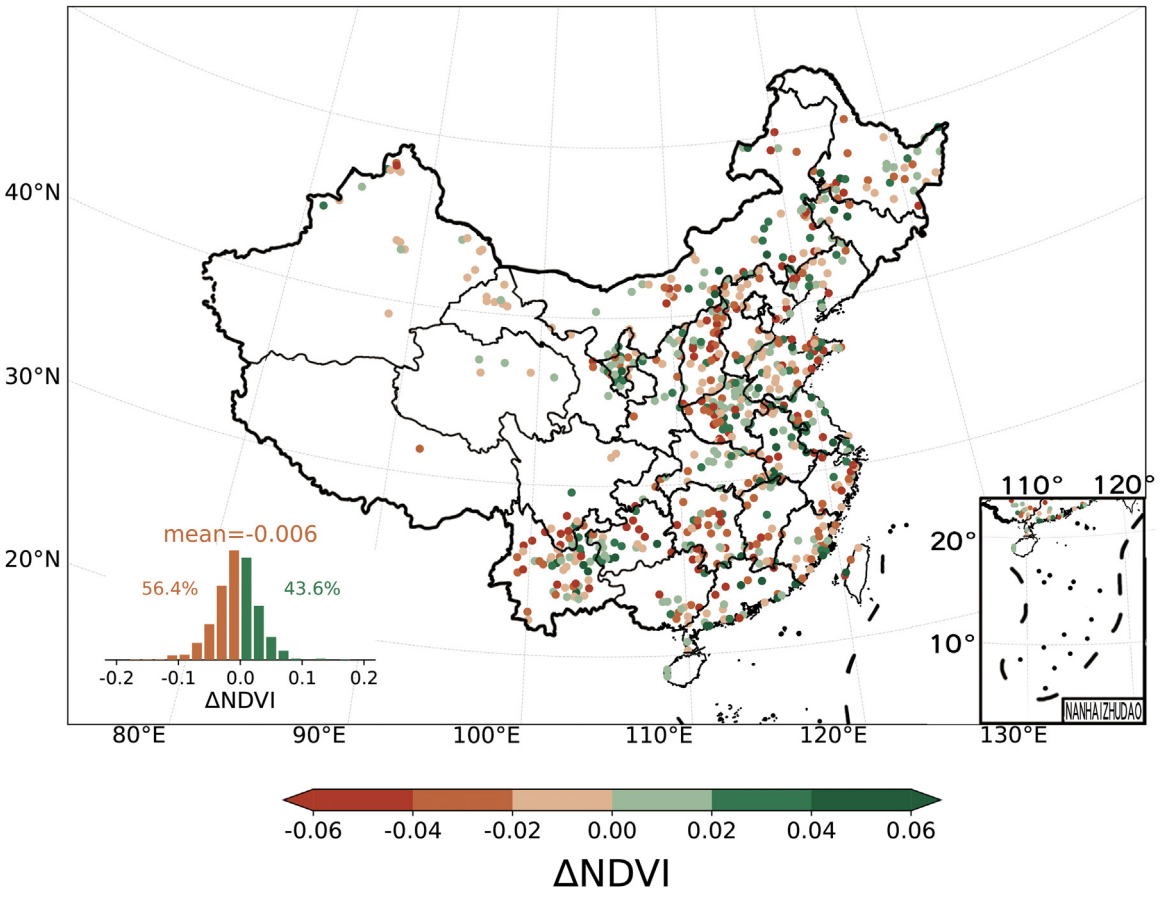

Fig. 5. Wind farm impacts on peak NDVI (ΔNDVI). The insets show the histogram of ΔNDVI for 675 wind farms with mean values and percentages of positive (green) and negative (red) values. The ΔNDVI was calculated based on the average of MODIS Aqua and Terra satellite products.

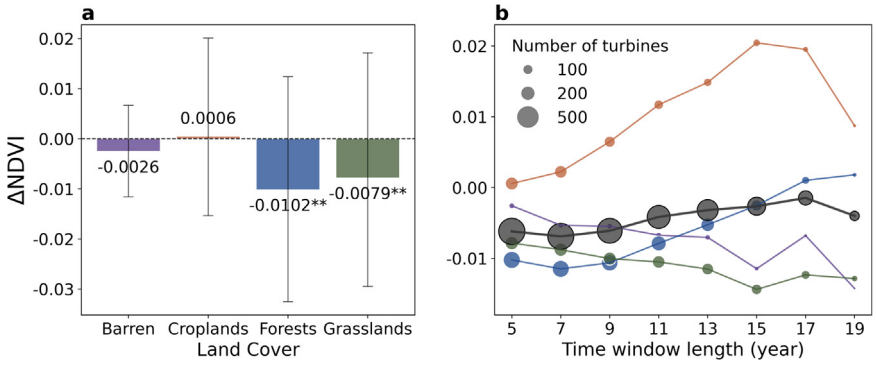

Fig. 6. Wind farm impacts on vegetation under different land cover types (a) and by different time window lengths (b). Asterisks in panel a indicate statistical significance using a *t*-test, with ** for $p < 0.01$, * for $p < 0.05$, and no mark for the insignificant ones. Grey error bars in panel a represent the interquartile range. The line in panel b represents the average ΔNDVI of all samples under a specific time window length. The size of the scatter points in panel b represents the number of samples, ranging from 4 to 675.

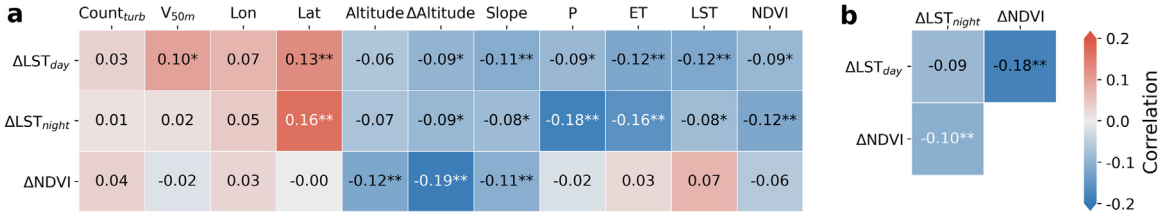

Fig. 7. Pearson correlations between wind farm impacts and environmental factors (a) and correlations of wind farm impacts among themselves (b). Environmental variables include turbine counts ($Count_{turb}$), 50 m wind velocity (V_{50m}), longitude (Lon), latitude (Lat), altitude (Altitude), altitude difference (ΔAltitude) between WFs and NWF region, slope (Slope), precipitation (*P*), evapotranspiration (ET), annual LST (LST), and annual NDVI (NDVI). Asterisks indicate statistical significance using a *t*-test, with ** for $p < 0.01$, * for $p < 0.05$, and no mark for the insignificant ones.

ular, the negative correlation with altitude indicates that LST decreases with increasing elevation (Ghaderpour et al., 2024). This altitude dependence means that wind farms located at higher elevations would show weaker warming effects. Moreover, the high surface roughness of lush vegetation and the high background TKE in complex terrain dampen the influence of turbine-induced roughness and turbulence, thus weakening the warming effect (Xia et al., 2016). The nighttime ΔLST also showed significant negative correlations with evapotranspiration (−0.12), precipitation (−0.09), and LST (−0.08), indicating the role of large-scale climate conditions, as wind farms had a stronger warming impact in cooler and drier climates. Since nighttime ΔLST (−0.16) and most influencing factors covaried with latitude, we used partial correlation, controlling for latitude, and found that precipitation remained a significant influencing factor (−0.08), while LST (0.10) shifted from a negative to a positive correlation (Table S3 in the Supplementary materials). Therefore, precipitation emerged as a robust factor, indicating a stronger nighttime warming effect in drier areas, such as the desert of northwestern China (Liu et al., 2022). The quick decrease in the desert LST at night may create a more stable near-surface atmospheric layer, which favors the formation of turbine-induced night warming (Baidya Roy and Traiteur, 2010; Loriaux et al., 2017).

For the vegetation effect, ΔNDVI showed significant negative correlations with altitude (−0.09), altitude difference (−0.15), and slope (−0.08), indicating wind farms in more complex terrain may lead to greater vegetation decline. It may also be associated with the covariation between land cover type and topography. For example, forests are typically located in mountainous areas; wind farms built there would cause a more significant decrease in vegetation (Fig. 6). In contrast, wind farms in barren lands, croplands, and grasslands were often located in flatter areas with high levels of human disturbance. The distribution of land cover types contributes to spatial variations in wind farm impacts as land cover covaries with geographical and climatic conditions.

The impacts on vegetation and LST had interactions (Fig. 7b), as indicated by significant correlations between ΔNDVI and daytime ΔLST (−0.18) and nighttime ΔLST (−0.10). Vegetation decline may further exacerbate warming at wind farms by reducing evapotranspiration cooling.

4. Discussion

4.1. Comparison with the literature

Our assessment of 675 wind farms provides a comprehensive view of their impacts in China, with an improved representativeness than previous studies. We compared the wind farm impacts estimated in our study with those reported in the literature for the same location, based on remote sensing (Table 1). Our estimation was generally consistent with most reported wind farm impacts. Some discrepancies were expected in the comparison because different wind turbine locations and quantification methods were used.

4.2. Mechanisms of wind farm impacts

Our analyses, based on a large sample of wind farms in China, revealed prominent night warming impacts on LST in most seasons, except summer. In contrast, the significant daytime cooling effect was only evident in spring (Fig. S4). These diurnally asymmetric LST impacts result from changes in land and atmosphere interactions induced by wind farms. In general, wind turbines increase surface roughness (Kirk-Davidoff and Keith, 2008). Operational wind turbines absorb the momentum of the airflow and convert a small portion of it into turbulence (Xia et al., 2016). This causes mixing in the atmospheric boundary layer, thereby altering heat and moisture exchange between the land and the atmosphere (Armstrong et al., 2014; Baidya Roy and Traiteur, 2010; Zhou et al., 2012). Consequently, the wind farm impacts on LST depend on atmospheric conditions, including stability, wind speed, and turbulent kinetic energy. Under stable atmospheric conditions (e.g., at night), the blades bring higher-potential-temperature air from higher altitudes to the surface, causing the surface to warm (Zhou et al., 2012). The strength of turbine-induced turbulence relative to the background turbulent kinetic energy explains the diurnal and seasonal variations in LST effects (Xia et al., 2016). During the daytime, the wind turbine mixing transports cooler air from above to the ground, but this is diluted by the strong background TKE, resulting in a weak impact. Wind speed in this study did not show a significant spatial relationship with the LST effect, possibly due to other confounding factors. Further investigation can focus on the temporal relationship between wind farm impacts and the vertical temperature profile to explore their dynamics at different time scales.

Regarding the impacts on vegetation, approximately 56 % of the 675 wind farms in China have inhibited local vegetation, particularly in forests and grasslands. The adverse effect on vegetation can be caused by vegetation removal during construction or by the microclimate changes induced by the wake effect (reduced wind speed) (Diffendorfer et al., 2022). Vegetation removal is a more likely explanation, as the detected vegetation loss is mainly limited to the wind farm areas (Fig. S6 in the Supplementary materials). Since there is a close relationship between LST and NDVI (Ghaderpour et al., 2024; Mortier et al., 2024), a decrease in NDVI could, in turn, amplify wind farm-induced warming during both day and night (Fig. 7b). Additionally, the coarse spatial resolution of MODIS NDVI data (1 km) can mitigate the detected impact on vegetation. The vegetation impact was stronger (0.127–0.232 at the 0–30 m buffer area) when using NDVI data at a 30 m resolution (Ma et al., 2023). Over time, vegetation may recover from wind farm construction and show positive changes, as observed in 44 % of wind farms.

4.3. Contribution of land cover dependency in latitudinal variations

The land-cover dependency is a prominent feature of wind farm impacts, reflecting complex and heterogeneous interactions between LST and land cover with different surface properties (e.g., roughness, albedo) (Ghaderpour et al., 2024). For nighttime LST impacts, the night warming decreased from barren lands, croplands, and grasslands to forests, similar to the rankings of 319 wind farms in the United States (croplands: 0.17 °C > grasslands: 0.11 °C > forests: −0.01 °C, with the absence of barren lands) (Qin et al., 2022). The roughness changes caused by wind farms relative to the underlying land cover correspond to the consequent LST impacts. For example, forests have higher roughness, and wind farms built in forests exhibited weaker ΔLST because of smaller roughness changes. In contrast, wind farms built on bare lands exhibited the strongest warming, probably due to the largest roughness changes. Another study of 76 wind farms in northern China found a higher warming in grasslands (0.141 °C) than in croplands (−0.004 °C) (Liu et al., 2023). The different rankings were likely due to the use of different wind farm samples in each study. According to our results, differences in night LST impacts between croplands and grasslands were insignificant (independent sample t-test, $p = 0.338$). Numerical model simulations help clarify the mechanisms of how wind farm impacts vary under different land surface conditions (Wang et al., 2019).

Another key feature of wind farm-induced nighttime warming is the latitudinal distribution. Fig. 2d shows that the nighttime warming effects of wind farms increased significantly with latitude. Because of the inter-dependence between latitude, wind farm impacts, and land cover distributions (e.g., more barren lands and grasslands in the north, while more forests in the south) (Fig. 8a), the latitudinal pattern of nighttime LST effects may result from the latitudinal distribution of land cover types. We decomposed the latitudinal nighttime ΔLST into contributions of land cover distribution (Fig. 8b) and other factors (Fig. 8c). The ΔLST contribution from land cover distribution exhibited evident latitude dependency ($p < 0.01$), suggesting the latitudinal distribution of land cover is the primary factor in the latitudinal ΔLST ($r = 0.54$; Fig. 8c) that is not

Table 1
Comparison of annual mean land surface temperature (LST) effects estimated in this study with the literature at the same wind farms. For studies including multiple wind farms, the average impacts within the spatial extent of our wind farms were calculated.

Wind farms*	Time range	Land cover	ΔLST in the literature (°C)		ΔLST in this study (°C)	
			Daytime	Nighttime	Daytime	Nighttime
Northern China (76 farms)[1]	2001–2018 (growing season)	Croplands, grasslands	0.060	0.111	0.051	0.111
Northwestern China (16 farms)[2]	2001–2018	Desert	0.250 ± 0.519	0.237 ± 0.146	0.109	0.206
Zhangbei Plain[3]	2016 (Apr, Jul, Oct, Jan)	/	0.15	0.3	0.10	0.23
Guazhou, Gansu[4]	2005–2012	Barren Gobi Desert	−0.18	0.37	−0.11	0.11
Shangyi, Hebei[5]	2003–2018	Semi-arid prairie	0.37 (daily)		0.12 (daily)	
Shangyi, Hebei[6]	2001–2019	Croplands, grasslands	−0.58	0.46	0.13	0.11
Inner Mongolia[7]	1990–2020	Forests, grasslands, croplands	0.14 ± 2.34	0.23 ± 1.62	0.05*	0.07*
Inner Mongolia[8]	2003–2022 (growing season)	Grasslands	−0.032 ± 0.608	0.067 ± 0.206		
Bashang, Hebei[9]	2003–2014	Croplands, grasslands	0.45–0.65	0.15–0.18	0.25	0.13

* If our study did not include the identical wind turbines, the mean impact was calculated from surrounding wind farms for comparison. If applicable, the reported range of wind farm impact in the literature is shown. References of each wind farm are noted as: 1 (Liu et al., 2023), 2 (Liu et al., 2022), 3 (Wang et al., 2019), 4 (Chang et al., 2016), 5 (Liu et al., 2021), 6 (Luo et al., 2021), 7 (Liu et al., 2024), 8 (Su et al., 2024), 9 (Tang et al., 2017). For the Shangyi wind farm in Hebei, the merged columns mean that only the daily average results are reported.

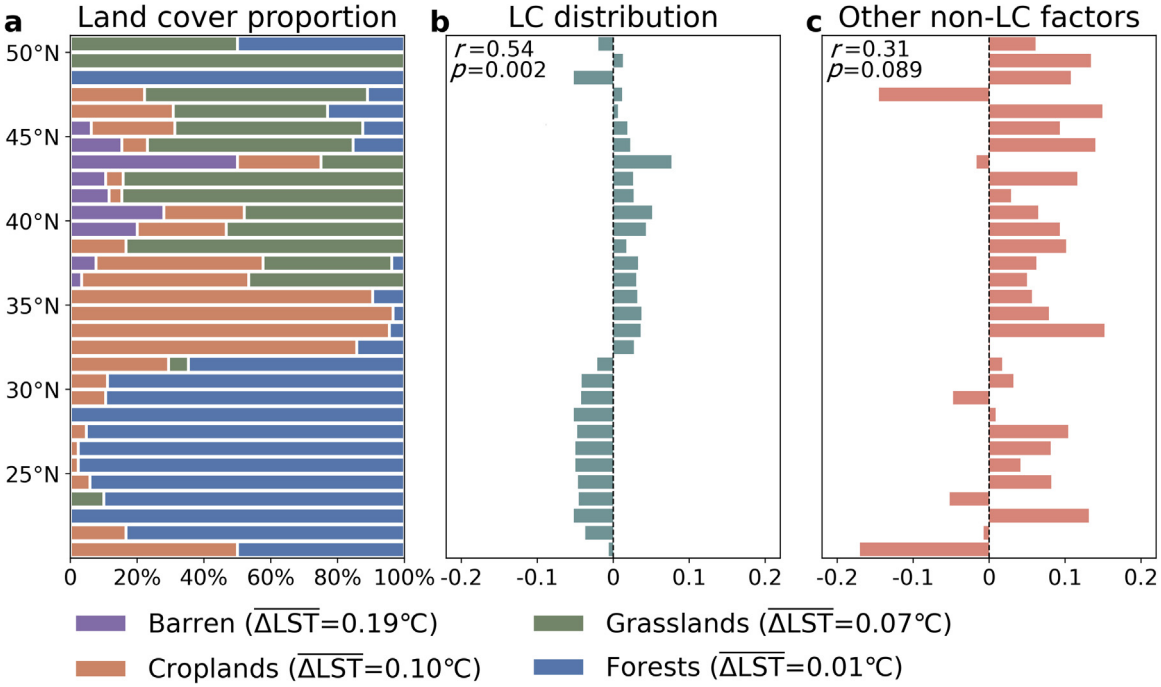

Fig. 8. Attribution of the latitudinal distribution of wind farm impacts on nighttime LST. (a) Latitudinal distribution of land cover. (b-c) The decomposed latitudinal contribution of land cover (LC distribution) (b) and other non-land cover factors (c).

directly included in the correlation analysis. ΔLST contributions from other factors combined were less important (r = 0.31) (Fig. 8c).

Wind farm characteristics, such as wind farm size as measured by the number of turbines, were identified as an important factor in previous studies (Qin et al., 2022). Although night warming tends to increase for larger wind farms, wind farm size was not a significant factor in our correlation analysis. This may be because most wind farms in this study are relatively small in size (half of them are ≤ 35 turbines) (Fig. S7a in the Supplementary materials). Further, wind farm size varied across land cover types, potentially contributing to spatial variation (Fig. S7b). For example, wind farms were generally large on barren land (average size = 259) but smaller in forests (average size = 53). When controlling wind farm size in small ranges, the nighttime LST impact in most cases remained strong on barren land and weak on forests (Fig. S7c). These results demonstrate that wind farm size is not a major factor in determining the differences in LST impacts across different land cover types.

4.4. Uncertainties and limitations

There are uncertainties and limitations in quantifying wind farm impacts. The quantification method assumes similar background climate changes between wind farms and their adjacent 8–10 km buffer zone and attributes their differences to wind farm impacts. In reality, the validity of this assumption may be affected by spatial heterogeneity and temporal variability in climate change, as well as unaccounted local factors unrelated to wind farms. For example, the uneven spatial distribution of grazing activities in grasslands and the frequent changes in crop

types and cropland management practices (such as irrigation and fertilization) may confound the assumptions. Although the distance of 8–10 km to WF is considered to be under minimal wind farm impacts, the downwind influence of some massive wind farms may extend beyond 8–10 km, whose impacts could be underestimated in our analysis.

We used only MODIS land cover data from 2019 to classify the dominant land cover type for each wind farm, thereby omitting land cover changes and mixed land cover types. However, the omitted land changes are expected to have a limited influence on our results because, within the relatively short time window, the scattered land cover changes near the wind farm and non-wind farm area would not be large enough to alter the primary land cover type and the LST temporal changes of the WF and NWF areas. Given the heterogeneous nature, confounding effects from secondary or mixed land cover would likely be canceled out when averaging across turbines within an individual wind farm and across the 675 wind farm samples. This is also the strength of a large-sample analysis, which reduces the influence of unobserved local factors.

Uncertainties and observational errors exist in the data. The LST product is available for clear-sky conditions. This means the estimated LST impact applies only to sunny conditions, but not cloudy conditions. Regarding spatial scale, the coarse spatial resolution of MODIS NDVI data may mask small-scale changes and underestimate vegetation change, as more substantial vegetation changes are observed using Landsat datasets with higher resolution (Ma et al., 2023). To reduce the uncertainty associated with relying on a single dataset, we compared the wind farm impacts on annual mean LST, peak NDVI, and peak enhanced vegetation index (EVI) from MODIS Aqua and Terra, obtaining similar results across the datasets (Table S4 in the Supplementary materials). Some differences were observed in the vegetation impact on grasslands: Aqua data showed a significant decline (−0.011, 38.9 % positive, $p < 0.01$), whereas Terra data showed no significant impacts (−0.005, 43.4 % positive, $p = 0.235$).

Wind farm construction is a continuous process spanning several years, with new turbines built annually. Since this study used wind turbines identified in 2019, this dynamic process would affect the estimated wind farm impacts within a 5-year window. To test the sensitivity of the main results, we chose alternative window lengths ranging from 5 to 19 years and found that the conclusions were generally similar. The LST impacts increased with a longer time window length (Table S5 in the Supplementary materials), presumably due to the addition of newly installed turbines in subsequent years. Regarding the impact on vegetation, the longer the time window, the weaker the adverse effects, suggesting vegetation recovery. These results indicate that the detection of wind farm impact is influenced by the chosen time period, which may explain the different findings in the literature.

5. Conclusions

This comprehensive assessment, based on 675 wind farms, provides new observational evidence on the impacts of wind farms on land surface temperature and local vegetation in China. Our results indicated significant warming impacts on LST induced by wind farms at night and more heterogeneous and weaker impacts during the daytime. Wind farms had an overall adverse impact on vegetation owing to infrastructure construction. Still, the declining vegetation may recover over time in forests and croplands. Given the diverse land cover properties, such as roughness or vegetation conditions, there were considerable differences in wind farm impacts across land cover types. These differences included the strong nighttime warming and minimal vegetation impact on barren lands, versus the weak nighttime warming and intense vegetation loss in forests. The wind farm-induced LST and vegetation impacts can reinforce each other. This impact interaction and land-cover dependence contribute to the heterogeneous spatial pattern of wind farm impacts, which neither wind farms nor environmental factors can fully explain. Since our study focused on onshore wind farms, the impacts of the expanding offshore wind farms still need to be explored. In the future, remote sensing assessments like this can be combined with numerical simulations to advance the mechanistic understanding of wind farm impacts, helping to inform the environmental consequences of wind energy development and guide the planning of renewable energy at low environmental cost.

Data availability statement

All data used in this study are publicly available except wind turbine location data. The detailed information of 675 wind farms used in this analysis and their impact summary can be found in the supplementary file Table_S1.xlsx. The code and data that support the findings of this study are openly available at Figshare (https://doi.org/10.6084/m9.figshare.30951173).

Declaration of competing interests

The authors declare that they have no known competing financial interests or personal relationships that could have appeared to influence the work reported in this paper. Yan Li is an Editorial Board Member for this journal and was not involved in the editorial review or the decision to publish this article.

CRediT authorship contribution statement

Ziyan Li: Writing – original draft, Visualization, Validation, Software, Methodology, Formal analysis. **Yan Li:** Writing – review & editing, Resources, Methodology, Funding acquisition, Conceptualization. **Yingzuo Qin:** Writing – review & editing, Software, Methodology. **Laibao Liu:** Writing – review & editing. **Eviatar Bach:** Writing – review & editing. **Alona Armstrong:** Writing – review & editing. **Guoqing Li:** Writing – review & editing. **Mingquan Li:** Writing – review & editing. **Zheng Wang:** Writing – review & editing. **Yongqing Bai:** Data curation. **Zhengchao Chen:** Data curation.

Acknowledgements

This study is supported by the National Key R&D Program of China (Grant No. 2024YFF0811100), the National Natural Science Foundation of China (Grant No. 41901115), and the 111 Project of China (Grant No. B23027). We thank Yuehan Yu for her help with the graphical abstract and proofreading.

Supplementary materials

Supplementary material associated with this article can be found, in the online version, at doi:10.1016/j.geosus.2026.100460.

References

Aksoy, T., Cetin, M., Cabuk, S.N., Kurkcuoglu, M.A.S., Ozturk, G.B., Cabuk, A., 2023. Impacts of wind turbines on vegetation and soil cover: a case study of Urla, Cesme, and Karaburun Peninsulas, Turkey. Clean Technol. Environ. Policy 25 (1), 51–68. doi:10.1007/s10098-022-02387-x.

Armstrong, A., Waldron, S., Whitaker, J., Ostle, N.J., 2014. Wind farm and solar park effects on plant-soil carbon cycling: uncertain impacts of changes in ground-level microclimate. Glob. Change Biol. 20 (6), 1699–1706. doi:10.1111/gcb.12437.

Baidya Roy, S., Traiteur, J.J., 2010. Impacts of wind farms on surface air temperatures. Proc. Natl. Acad. Sci. U.S.A. 107 (42), 17899–17904. doi:10.1073/pnas.1000493107.

Chang, R., Zhu, R., Guo, P., 2016. A case study of land-surface-temperature impact from large-scale deployment of wind farms in China from Guazhou. Remote Sens. 8 (10), 790. doi:10.3390/rs8100790.

Diffendorfer, J.E., Vanderhoof, M.K., Ancona, Z.H., 2022. Wind turbine wakes can impact down-wind vegetation greenness. Environ. Res. Lett. 17 (10), 104025. doi:10.1088/1748-9326/ac8da9.

Fiedler, B.H., Bukovsky, M.S., 2011. The effect of a giant wind farm on precipitation in a regional climate model. Environ. Res. Lett. 6 (4), 045101. doi:10.1088/1748-9326/6/4/045101.

Gelaro, R., McCarty, W., Suárez, M.J., Todling, R., Molod, A., Takacs, L., Randles, C.A., Darmenov, A., Bosilovich, M.G., Reichle, R., Wargan, K., Coy, L., Cullather, R., Draper, C., Akella, S., Buchard, V., Conaty, A., da Silva, A.M., Gu, W., Kim, G.K., Koster, R., Lucchesi, R., Merkova, D., Nielsen, J.E., Partyka, G., Pawson, S., Putman, W., Rienecker, M., Schubert, S.D., Sienkiewicz, M., Zhao, B., 2017. The modern-era retrospective analysis for research and applications, version 2 (MERRA-2). J. Clim. 30 (14), 5419–5454. doi:10.1175/JCLI-d-16-0758.1.

Ghaderpour, E., Mazzanti, P., Bozzano, F., Scarascia Mugnozza, G., 2024. Trend analysis of MODIS land surface temperature and land cover in central Italy. Land 13 (6), 796. doi:10.3390/land13060796.

Hersbach, H., Bell, B., Berrisford, P., Hirahara, S., Horányi, A., Muñoz-Sabater, J., Nicolas, J., Peubey, C., Radu, R., Schepers, D., Simmons, A., Soci, C., Abdalla, S., Abellan, X., Balsamo, G., Bechtold, P., Biavati, G., Bidlot, J., Bonavita, M., De Chiara, G., Dahlgren, P., Dee, D., Diamantakis, M., Dragani, R., Flemming, J., Forbes, R., Fuentes, M., Geer, A.L., Haimberger, L., Healy, S., Hogan, R.J., Hólm, E., Janisková, M., Keeley, S., Laloyaux, P., Lopez, P., Lupu, C., Radnoti, G., de Rosnay, P., Rozum, I., Vamborg, F., Villaume, S., Thépaut, J.N., 2020. The ERA5 global reanalysis. Q.J.R. Meteorol. Soc. 146 (730), 1999–2049. doi:10.1002/qj.3803.

Hou, C.Z., Xu, Z.W., Karnauskas, K.B., Huang, D.Q., Lu, H.Y., 2025. Detecting and calibrating large biases in global onshore wind power assessment across temporal scales. Nat. Commun. 16 (1), 3775. doi:10.1038/s41467-025-59195-2.

Kirk-Davidoff, D.B., Keith, D.W., 2008. On the climate impact of surface roughness anomalies. J. Atmos. Sci. 65 (7), 2215–2234. doi:10.1175/2007JAS2509.1.

Li, L., Ma, W.J., Duan, X.Y., Wang, S., Wang, Q., Gu, H.L., Wang, J.S., 2024. Effects of wind farm construction on soil nutrients and vegetation: a case study of Linxiang wind farm in Hunan Province. Sustainability 16 (15), 6350. doi:10.3390/su16156350.

Li, Y., Kalnay, E., Motesharrei, S., Rivas, J., Kucharski, F., Kirk-Davidoff, D., Bach, E., Zeng, N., 2018. Climate model shows large-scale wind and solar farms in the Sahara increase rain and vegetation. Science 361 (6406), 1019–1022. doi:10.1126/science.aar5629.

Liu, L.Y., Liu, P.T., Yu, J.W., Feng, G., Zhang, Q., Svenning, J.-C., 2024. Wind farms increase land surface temperature and reduce vegetation productivity in the Inner Mongolia. Geogr. Sustain. 5 (3), 319–328. doi:10.1016/j.geosus.2024.01.007.

Liu, N.J., Zhao, X., Zhang, X., Zhao, J.C., Wang, H., Wu, D.H., 2022. Heterogeneous warming impacts of desert wind farms on land surface temperature and their potential drivers in Northern China. Environ. Res. Commun. 4 (10), 105006. doi:10.1088/2515-7620/ac9bd7.

Liu, N., Zhao, X., Zhang, X., Zhao, J., Wang, H., Wu, D., 2023. Remotely sensed evidence of the divergent climate impacts of wind farms on croplands and grasslands. Sci. Total Environ. 905, 167203. doi:10.1016/j.scitotenv.2023.167203.

Liu, Y.H., Dang, B., Xu, Y.M., Weng, F.Z., 2021. An observational study on the local climate effect of the Shangyi wind farm in Hebei Province. Adv. Atmos. Sci. 38 (11), 1905–1919. doi:10.1007/s00376-021-0290-0.

Loriaux, J.M., Lenderink, G., Siebesma, A.P., 2017. Large-scale controls on extreme precipitation. J. Clim. 30 (3), 955–968. doi:10.1175/JCLI-d-16-0381.1.

Luo, L.H., Zhuang, Y.L., Duan, Q.T., Dong, L.X., Yu, Y., Liu, Y.H., Chen, K.R., Gao, X.Q., 2021. Local climatic and environmental effects of an onshore wind farm in North China. Agric. For. Meteorol. 308-309, 108607. doi:10.1016/j.agrformet.2021.108607.

Ma, B.R., Yang, J.H., Chen, X.H., Zhang, L.X., Zeng, W.H., 2023. Revealing the ecological impact of low-speed mountain wind power on vegetation and soil erosion in South China: a case study of a typical wind farm in Yunnan. J. Clean. Prod. 419, 138020. doi:10.1016/j.jclepro.2023.138020.

Miller, L.M., Keith, D.W., 2018. Climatic impacts of wind power. Joule 2 (12), 2618–2632. doi:10.1016/j.joule.2018.09.009.

Mortier, S., Hamedpour, A., Bussmann, B., Wandji, R.P.T., Latré, S., Sigurdsson, B.D., De Schepper, T., Verdonck, T., 2024. Inferring the relationship between soil temperature and the normalized difference vegetation index with machine learning. Ecol. Inform. 82, 102730. doi:10.1016/j.ecoinf.2024.102730.

Pan, Y., Archer, C.L., 2018. A hybrid wind-farm parametrization for mesoscale and climate models. Bound.-Layer Meteorol. 168 (3), 469–495. doi:10.1007/s10546-018-0351-9.

Qin, Y.Z., Li, Y., Xu, R., Hou, C.C., Armstrong, A., Bach, E., Wang, Y., Fu, B.J., 2022. Impacts of 319 wind farms on surface temperature and vegetation in the United States. Environ. Res. Lett. 17 (2), 024026. doi:10.1088/1748-9326/ac49ba.

Redmon, J., Divvala, S., Girshick, R., Farhadi, A., 2016. You only look once: unified, real-time object detection. In: 2016 IEEE Conference on Computer Vision and Pattern Recognition (CVPR). June 27–30, 2016. IEEE, Las Vegas, NV, USA, pp. 779–788. doi:10.1109/CVPR.2016.91.

Roy, S., Pacala, S., Walko, R., 2004. Can large wind farms affect local meteorology? J. Geophys. Res. Atmos. 109 (D19), D19101. doi:10.1029/2004JD004763.

Slawsky, L.M., Zhou, L.M., Roy, S.B., Xia, G., Vuille, M., Harris, R.A., 2015. Observed thermal impacts of wind farms over Northern Illinois. Sensors 15 (7), 14981–15005. doi:10.3390/s150714981.

Su, N., Li, X., Lyu, X., Dang, D., Liu, S., Zhang, C., 2024. Comprehensive assessment of the climatic and vegetation impacts of wind farms on grasslands: a case study in Inner Mongolia, China. J. Environ. Manage. 370, 122430. doi:10.1016/j.jenvman.2024.122430.

Tang, B.J., Wu, D.H., Zhao, X., Zhou, T., Zhao, W.Q., Wei, H., 2017. The observed impacts of wind farms on local vegetation growth in Northern China. Remote Sens. 9 (4), 332. doi:10.3390/rs9040332.

Urziceanu, M., Anastasiu, P., Rozylowicz, L., Sesan, T.E., 2021. Local-scale impact of wind energy farms on rare, endemic, and threatened plant species. PeerJ 9, e11390. doi:10.7717/peerj.11390.

Wang, G., Li, G.Q., Liu, Z., 2023. Wind farms dry surface soil in temporal and spatial variation. MethodsX 10, 102000. doi:10.1016/j.mex.2023.102000.

Wang, Q., Luo, K., Wu, C.L., Fan, J.R., 2019. Impact of substantial wind farms on the local and regional atmospheric boundary layer: case study of Zhangbei wind power base in China. Energy 183, 1136–1149. doi:10.1016/j.energy.2019.07.026.

World Wind Energy Association, 2025. WWEA Annual Report 2024: A Challenging Year for Windpower. https://wwindea.org/GlobalStatistics/. (accessed 12 March 2026).

Wu, X.L., Zhang, L.X., Zhao, C.F., Gegen, T., Zheng, C.W., Shi, X.Q., Geng, J., Letu, H., 2019. Satellite-based assessment of local environment change by wind farms in China. Earth Space Sci. 6 (6), 947–958. doi:10.1029/2019EA000628.

Xia, G., Zhou, L.M., Freedman, J.M., Roy, S.B., Harris, R.A., Cervarich, M.C., 2016. A case study of effects of atmospheric boundary layer turbulence, wind speed, and stability on wind farm induced temperature changes using observations from a field campaign. Clim. Dyn. 46 (7–8), 2179–2196. doi:10.1007/s00382-015-2696-9.

Xia, Z.L., Li, Y.J., Guo, S.C., Zhang, X.G., Pan, X.Q., Fang, H., Chen, R.S., Du, P.J., 2025. Assessment of forest disturbance and soil erosion in wind farm project using satellite observations. Resour. Conserv. Recycl. 212, 107934. doi:10.1016/j.resconrec.2024.107934.

Xu, K., He, L.C., Hu, H.J., Liu, S., Du, Y.Y., Wang, Z.W., Li, Y., Li, L.Y., Khan, A., Wang, G.X., 2019. Positive ecological effects of wind farms on vegetation in China's Gobi desert. Sci. Rep. 9, 3901. doi:10.1038/s41598-019-42569-0.

Zhai, Y.C., Chen, X.H., Cao, X., Cui, X.H., 2024. Identifying wind turbines from multiresolution and multibackground remote sensing imagery. Int. J. Appl. Earth Obs. Geoinf. 126, 103613. doi:10.1016/j.jag.2023.103613.

Zhang, X., Wang, H.M., Shang, G.F., Sun, M.H., Yan, Z.H., Gao, Y.X., Yuan, Q.X., Zhang, C., 2023. Impact of wind farms on local land surface temperature in Qinghai Province, China. Int. J. Remote Sens. 45 (19–20), 7318–7338. doi:10.1080/01431161.2023.2211207.

Zhou, L.M., Tian, Y.H., Baidya Roy, S., Dai, Y.J., Chen, H.S., 2013. Diurnal and seasonal variations of wind farm impacts on land surface temperature over western Texas. Clim. Dyn. 41 (2), 307–326. doi:10.1007/s00382-012-1485-y.

Zhou, L.M., Tian, Y.H., Baidya Roy, S., Thorncroft, C., Bosart, L.F., Hu, Y.L., 2012. Impacts of wind farms on land surface temperature. Nat. Clim. Chang. 2 (7), 539–543. doi:10.1038/nclimate1505.